Geophysical Research Letters

RESEARCH LETTER
10.1029/2022GL099999

Key Points:

- A bright meteor event near Granada has been recorded at 44 seismic stations at local distances
- Seismic location of the terminal burst using the ERA5 atmospheric model agrees with triangulation from regional meteor cameras
- Waveforms show large differences between nearby stations, suggesting an important imprint of local coupling and multipathing effects

Supporting Information:

Supporting Information may be found in the online version of this article.

Correspondence to:

D. Stich,
stich@ugr.es

Citation:

Stich, D., Casado Rabasco, J., Madiedo, J. M., Guerrero Rascado, J. L., & Morales Soto, J. (2022). Seismic observation and location of a meteor burst from a dense station deployment in southern Spain. *Geophysical Research Letters*, *49*, e2022GL099999. https://doi.org/10.1029/2022GL099999

Received 6 JUL 2022
Accepted 11 DEC 2022

Author Contributions:

Conceptualization: Daniel Stich, Jose Morales Soto
Data curation: Jose Morales Soto
Formal analysis: Daniel Stich, Josué Casado Rabasco, José María Madiedo, Juan Luis Guerrero Rascado
Methodology: Josué Casado Rabasco
Validation: Josué Casado Rabasco
Visualization: Daniel Stich, Josué Casado Rabasco
Writing – original draft: Daniel Stich, Josué Casado Rabasco

Seismic Observation and Location of a Meteor Burst From a Dense Station Deployment in Southern Spain

Daniel Stich[1,2], Josué Casado Rabasco[1,3], José María Madiedo[4], Juan Luis Guerrero Rascado[5,6], and Jose Morales Soto[1,2]

[1]Instituto Andaluz de Geofísica, Universidad de Granada, Granada, Spain, [2]Departamento de Física Teórica y del Cosmos, Universidad de Granada, Granada, Spain, [3]Department of Cartographic and Terrain Engineering, Universidad de Salamanca, Ávila, Spain, [4]Instituto de Astrofísica de Andalucía (IAA-CSIC), Granada, Spain, [5]Departamento de Física Aplicada, Universidad de Granada, Granada, Spain, [6]Instituto de Investigación del Sistema Tierra en Andalucía (IISTA-CEAMA), Granada, Spain

Abstract A meteor event on 11 December 2016 in southern Spain was accompanied by an audible boom and felt vibrations. Acousto-seismic coupling of the near-field pressure wave has been recorded by an unusually large number of 44 local seismic stations. Considering the ERA5 atmospheric temperature and wind speed model, we can attribute the seismic detections to a point source at 38 km height, coincident with the most luminous fragmentation event recorded by meteor cameras. We show and analyze waveforms, spectrograms and signal polarization along a dense, temporary broadband transect in the area. Seismic records show important differences between them, like large variability in polarization, amplitudes and frequency content, emphasizing the role of local effects. The duration and complexity of waveforms can be attributed to path and site effects, including multipathing through small-scale atmospheric heterogeneity and scattering of the incoming acoustic wavefield at local topography.

Plain Language Summary The evening of 11 December 2016, a bright meteor was observed in southern Spain, followed by an audible boom and felt vibrations. The vibrations were recorded at 44 seismometers in a $\sim 110 \times 100$ km^2 area. In order to locate the signal origin, we consider the atmospheric temperature and wind speed conditions at that time, and find that the wave arrival times are consistent with a source at 38 km height. The source can be associated with the principal explosion event of the meteor recorded by the cameras. A special aspect of this meteor fall is the density of the seismic observations, revealing large variability of the recordings at nearby stations. The observations suggest that the complexity of recorded waveforms is driven by the small-scale atmospheric structure, local topography and obstacles around the recording stations, as well as the peculiarities of ground coupling of atmospheric acoustic waves.

1. Introduction

The evening of 11 December 2016, near 22:25 local time (21:25 UTC), a meteor event with absolute magnitude $m = -17$ was observed from most of Spain. The event was recorded by meteor observing stations operating at different astronomical observatories in southern Spain (Madiedo, 2017). According to reports in news and social media, the meteor event produced a bright, white light in the night sky for several seconds, and was widely heard and felt. Eyewitness accounts mention an audible boom, ground vibration or tremor, and windows rattling at several places in the province of Granada. Many people have mistaken these vibrations for a weak earthquake. The testimonies point to the arrival of pressure waves on the ground. Such sound and infrasound signals are originated by the interaction between the atmosphere and the meteoroid, and might be related to the shock wave from the meteoroid passage at hypersonic speed, or to an explosive fragmentation event induced by frictional heating of the meteoroid in the atmosphere (e.g., Ceplecha et al., 1998; Edwards et al., 2008; Le Pichon et al., 2010).

Atmospheric acoustic signals from meteor falls, sonic booms, atmospheric explosions and other sources of sound and infrasound are partially converted into seismic waves at the Earth's surface, and may be detected by seismometers (e.g., Cates & Sturtevant, 2002; Edwards et al., 2007; Kanamori et al., 1991; Schneider et al., 2018; Walker et al., 2010). Given the prevalence of seismic instrumentation compared to infrasound sensors, seismograms often constitute the majority of available recordings for meteor events. Energetic events like the 2013 Chelyabinsk meteor terminal explosion can be recorded at seismic stations out to several 1000s km distance (Antolik et al., 2014; Heimann et al., 2013). Taking into account the atmospheric layering, distant observations are

Writing – review & editing: José María Madiedo, Juan Luis Guerrero Rascado, Jose Morales Soto

dominated by wave propagation through the high velocity acoustic channel in the upper stratosphere, with effective sound speed and ray paths being sensitive to the wind and temperature conditions (Cates & Sturtevant, 2002; Evers & Haak, 2007; Garcés et al., 1998; Hedlin et al., 2010; Le Pichon et al., 2010; Pierce, 2019; Virieux et al., 2004).

Within the troposphere, temperature and acoustic wave speed generally decrease with altitude, and atmospheric wavefields are refracted away from the Earth's surface. On the ground, direct acoustic arrivals from meteors can be observed only for relatively small distances, depending on atmospheric conditions and source height (Brown et al., 2003; McFadden et al., 2021). In consequence, meteor events that have been recorded in the near-field at several tens of local stations remain a rare exception (e.g., Arrowsmith et al., 2007; Ishihara et al., 2004). Here we report on the analysis of 44 detections at local seismic stations for the 2016, Granada meteor event. The recordings are used to distinguish between ballistic and explosive signals, locate the terminal explosion considering the actual atmospheric conditions, and compare the results to optical observations of the meteor entry. In addition, the density of the recording network will allow to recognize and evaluate the variability of the acoustic-seismic coupled wavefield over short distances.

2. Seismic Data of the 2016 Meteor Event

Following up the eyewitness reports of ground vibration, we examine regional seismograms for signs of airwave coupling to ground motion. We inspect waveforms from 68 seismic stations operated by the Instituto Andaluz de Geofísica (IAG) and Instituto Geográfico Nacional (IGN). This includes stations from the Spanish and Andalusian broadband networks, additional short period sensors and accelerometers, as well as a temporary station deployment south of Granada (Figure 1). The temporary deployment consists of a dense, E-W trending transect of 30 seismic broadband stations. We find a conspicuous signal between 21:28 and 21:32 UTC. The signal shows frequency content above 1 Hz, varying waveform complexity among the stations, and is present in vertical as well as in horizontal component seismograms, often associated with a distinct polarization of particle motion (Figures S1 and S2 in Supporting Information S1). The signal has low apparent velocity compared to waves from earthquakes, traveling across the network at ∼0.4 km/s. Such velocities near the acoustic wave speed corroborate the origin from an atmospheric perturbance. The signal is clearly visible at 44 local stations altogether.

Our detections include 29 out of 30 stations from the broadband transect, with the exception of one station affected by anthropogenic noise. The transect is characterized by dense station spacing of ∼3.5 km, and named the Tropical Profile (TP) as reference to the nearby Costa Tropical. All sites share uniform installation (sensor in vault on cemented base plate) and instrumentation (Nanometrics Trillium Compact 120 s three-component, broad-band sensors and 24 bit data logger Centaur 3, with sampling at 100 Hz). This allows for assessing the variability of acousto-seismic coupled waves over small distances, revealing significant differences between nearby stations in terms of signal duration, abruptness of the onset, or number and relative amplitude of prominent wave packages within the signal (Figures S1 and S2 in Supporting Information S1). A general characteristics of the recordings is the presence of pulses with displacement waveforms close to an inverted letter N, respectively a letter W in velocity waveforms (Figure 1). N-waves with compressive first motion are observed for meteor events, sonic booms, atmospheric explosions and thunder (e.g., Cates & Sturtevant, 2002; Kanamori et al., 1992; Lin & Langston, 2007). The abrupt shape of N-waves is inherited from the nearly instantaneous pressure change in the initial, nonlinear shock wave (Edwards et al., 2008; Pujol et al., 2005). We use velocity and displacement waveforms to assign arrival times at the onset of the principal wave package in the recordings.

The signal recorded across the local seismometer network could be related to one of the disintegration events visible on video recordings of the meteor fall, or to the ballistic shock wave from the entry in the atmosphere. A disintegration event acts essentially as an isotropic point source, radiating a wavefield with quasi-spherical geometry (Edwards & Hildebrand, 2004; Heimann et al., 2013). In this case, the arrival time isochrones on the ground are expected to show a circular pattern, although their symmetry can be distorted by the atmospheric conditions (D'Auria et al., 2006; McFadden et al., 2021). In turn, conical shock fronts produce hyperbolic or elliptical intersections with the ground, the latter being the common case for the hypersonic flight of meteoroids (velocities >10 km/s), with Mach angles smaller than the trajectory inclination (Edwards et al., 2008; Kanamori et al., 1991; Langston, 2004; Pujol et al., 2005; Tatum, 1999). The isochrones of wave arrivals for the 2016 meteor event are incomplete, reflecting a lack of local seismic stations to the northwest. Available isochrone sections

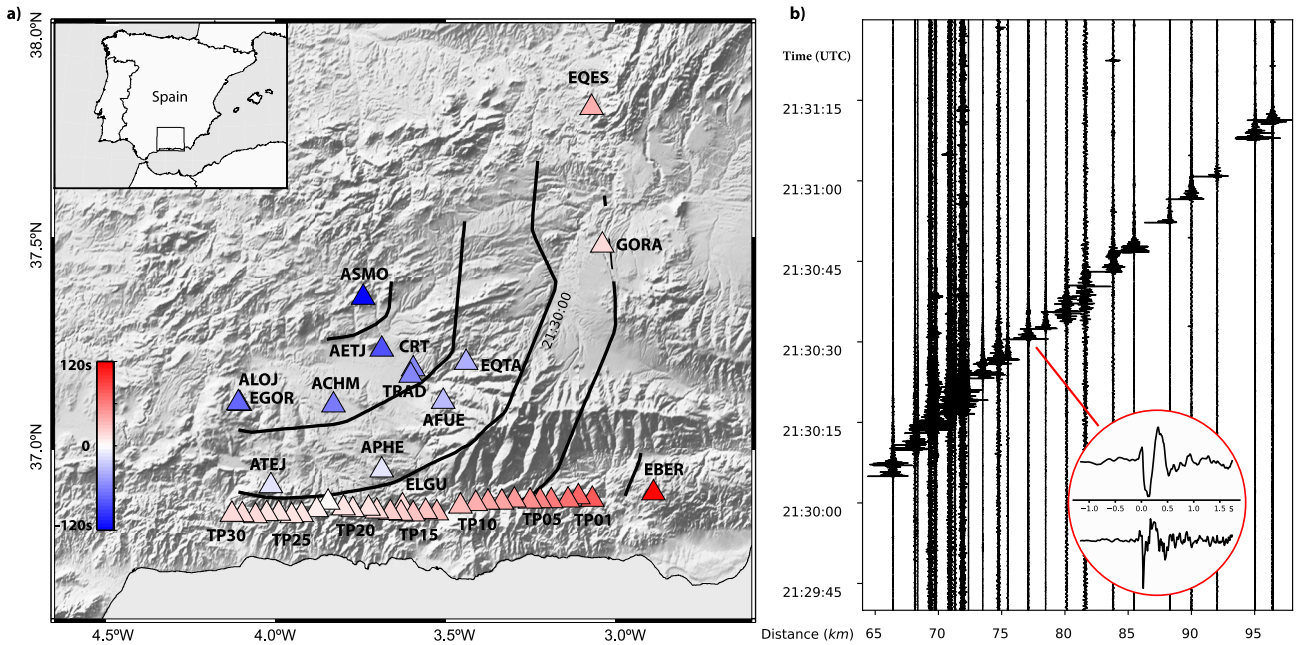

Figure 1. (a) Map of detections and arrival times of the pressure wave. Blue and red colors represent advance and delay of the arrival compared to a reference time of 21:30 UTC. Granada is located around stations CRT and TRAD. Arrival time isochrones (black) were interpolated from arrival picks using Delaunay Triangulation (Shewchuk, 1996). (b) Section of normalized, vertical component, velocity seismograms from the temporary station transect versus distance (horizontal distances to the calculated terminal burst location, see Section 3, seismograms are high-pass filtered at 1 Hz). The inlay shows an individual N-wave (displacement waveform, top) and W-wave (velocity waveform, bottom) arrival at station TP11.

describe circular arcs (Figure 1), with no notable elongation, suggesting an origin from a disintegration event. We will check this assumption again later by comparing the seismic location to camera recordings of the meteor fall.

3. Location of the Principal Fragmentation Event

Locating a source of acoustic waves in the atmosphere has to deal with a medium in motion, that is subject to rapid and relevant variations of parameters. The location and time of the seismically recorded fragmentation event is estimated from the atmospheric ray-tracing and source search algorithms implemented in the program package BAM (Bolide Acoustic Modeling, Edwards & Hildebrand, 2004; McFadden et al., 2021). Ray-tracing takes into account the horizontal wind speed and direction to compute the effective speed of wave propagation (Garcés et al., 1998; Pierce, 2019; Virieux et al., 2004). BAM uses particle swarm optimization for guided search of the source location, an algorithm where a population of candidate solutions moves semi-randomly through the solution space (Bonyadi & Michalewicz, 2017). For each candidate location, the ray trajectories and travel times are computed for all stations, the mean origin time is calculated and the mean absolute residual between predicted and picked arrivals is evaluated.

For modeling of wave propagation in the atmosphere, sufficiently accurate information about the instantaneous temperature and wind conditions is required. Atmospheric parameters are adopted from the ERA5 TP model for 11 December at 21:00 UTC, provided by the European Centre for Medium-Range Weather Forecasts (ECMWF Re-Analysis 5th Generation) (Hersbach et al., 2018). ERA5 reanalysis is based on assimilation, combining model data with observations from across the world into a globally complete and consistent data set, benefiting the quality of the reanalysis product. ERA5 has a vertical resolution of 37 pressure levels from 1,000 hPa to 1 hPa, along a grid with horizontal spacing of 0.25°. The adiabatic acoustic wave speed is obtained from temperature, approximating the atmosphere as an ideal gas with heat capacity ratio of 1.4 (Garcés et al., 1998). For raytracing, the geopotential data are converted to height and the wind speed and temperature models between source and receiver are interpolated using cubic splines (McFadden et al., 2021). At the time of the meteor entry, wind speed barely exceeds 10 m/s for the troposphere and most of the stratosphere, with a predominant direction to the south

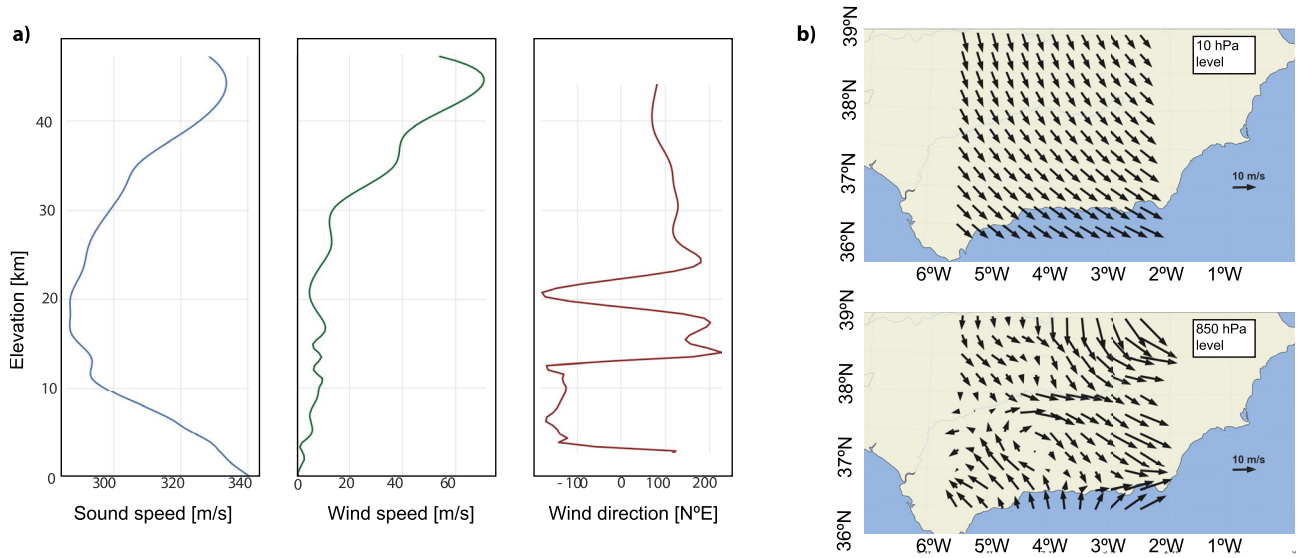

Figure 2. Atmospheric conditions according to the ERA5 model by the European Centre for Medium-Range Weather Forecasts (ECMWF). (a) Vertical profiles of adiabatic sound speed (calculated from ERA5 temperatures), wind speed and wind direction for coordinates 37.5°N, 4.0°W. (b) Modeled wind speed and direction for the lower troposphere (850 hPa) and mid stratosphere (10 hPa) from 36.5°N to 39.0°N and 5.5°W to 2.5°W.

and to the east at some levels (Figure 2). Such calm weather conditions are a fortunate situation for modeling, since they increase the predictability of atmospheric ray paths.

To locate the source, we explore a source volume between 4.25°W and 3.50°W, 37.25°N and 37.75°N, and from 20 to 50 km height, according to the pattern of travel time isochrones (Figure 1) and typical heights of meteor terminal explosions. Relative weights of 1.0 are assigned to permanent stations and weights of 0.2 to stations from the temporary transect, to prevent that the temporary deployment dominates the result. Inversion was performed for different populations of trial solutions in the particle swarm, and with fixed or free origin time. The particle swarm size was selected as 500 solutions, where convergence of the search appears robust for different random seeds. A fixed origin time at 21:25:47.3 UTC was tested, corresponding to the maximum luminosity recorded at meteor cameras (see below), but we found that treating the origin time as a free parameter gives equivalent results, and finally refrain from fixing the time. We admit in raytracing a significant vertical tolerance of 3 km, to cover diffracted arrivals (McFadden et al., 2021). Diffractions and creeping waves might reach the ground beyond the limit of the shadow zone predicted by geometrical ray theory (Pierce, 2019).

For this parameter settings, successful ray-tracing is possible to all 44 stations, yielding the source of the wavefield at 37.47°N, 3.92°W, altitude 38.4 km and origin time 21:25:47.2 UTC (Figure 3). The mean absolute travel time residual is 5.0 s, cumulating the uncertainties of atmospheric parameters, uncertainties in arrival times, diffraction effects, and mean absolute topography variations of ∼300 m among the stations. Residuals below 10 s are found for solutions within ∼5 km from the formally best solution (Figure 3). Ray paths become nearly horizontal at the eastern stations (GORA, EQES, EBER), indicating the proximity of the shadow zone. Locations further to the north, west and at lower altitude cannot reproduce detections at these stations, because rays are predicted to refract upward. The most distant detection corresponds to the stations of EBER, located in SE direction at horizontal distance of about 110 km from the source. We examined seismic stations at smaller distances in northern direction (JAND, azimuth N357°E, distance 83 km) and western direction (ESTP, N256°E, 87 km), without detection of the meteor signal, suggesting that the limit of the shadow zone is shifted toward the southeast, following the overall direction of the wind field. The inverted origin time compares favorably to the time of maximum luminosity, although the resolution of this parameter is low (±10 s, Figure 3).

The source location confirms the lack of azimuthal coverage and we cannot verify if isochrone fragments (Figure 1) correspond to spherical or conical wavefield geometry (Pujol et al., 2005; Tatum, 1999). Furthermore, the lack of short-distance observations (only two recordings at less than 40 km horizontal distance) prevents us from detecting an increase in apparent velocity underneath the source, as predicted for a spherical wavefield (D'Auria et al., 2006; McFadden et al., 2021). To corroborate the point source model, we check the consistency

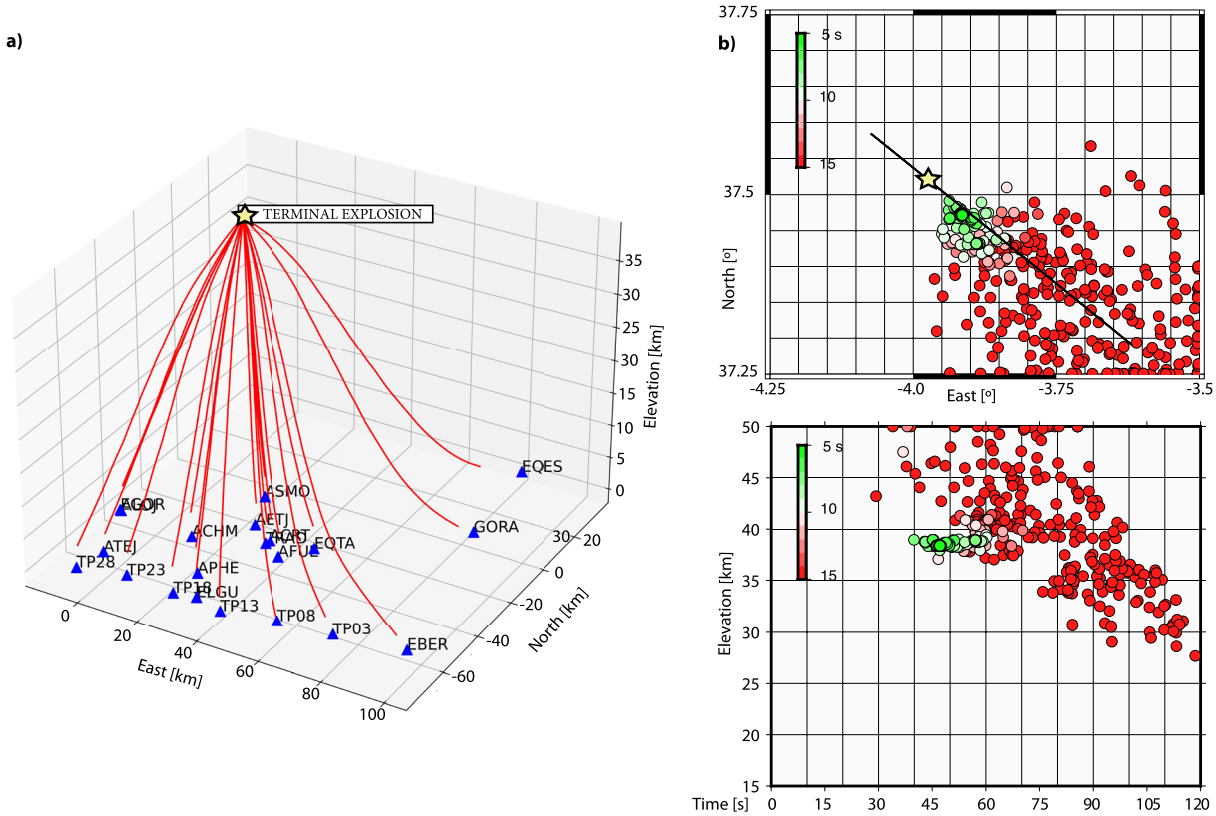

Figure 3. (a) Atmospheric ray paths between the terminal burst location and selected stations (for better visibility of the individual paths, only every fifth station of the broadband transect is shown). (b) Alternative solutions within the atmospheric volume explored by the search algorithm, color-coded according to the mean absolute traveltime error. The trajectory (black line) and terminal burst location (star) from optical observations (linear approximation) are plotted for comparison.

between the estimated time, height and coordinates to the meteor trajectory inferred from camera recordings. Especially source height allows a meaningful comparison, since traveltime isochrones align with the disintegration event for a spherical wavefield, but would align with the intersection of the meteor trail with the Earth's surface (height zero) for a conical wavefield.

The luminous phase of the 2016 event was recorded by five meteor cameras operating in the framework of the SMART project from the astronomical observatories of La Hita (Toledo), Sevilla, Calar Alto (Almería), Sierra Nevada and La Sagra (Granada) (Madiedo, 2017). On camera recordings we can observe the full meteor trajectory, including 13 distinct events of suddenly increasing brightness between 21:25:45.1 and 21:25:47.6 UTC. They suggest the presence of multiple fragmentation events, each producing a sudden increase in the meteoroid surface area that suffers ablation (Edwards et al., 2008; Heimann et al., 2013). As mentioned previously, the maximum luminosity corresponds to an event at 21:25:47.3 UTC, after which the brightness of the meteor significantly decreases for the last part of the luminous trail. Triangulation of the meteor trajectory places the start of the luminous phase at 37.290°N, 3.617°W and altitude 98.7 km, and its extinction at 37.585°N, 4.074°W, and altitude 18.5 km. This was calculated by employing the AMALTHEA software (Madiedo, 2014), which follows the planes intersection method to determine meteor atmospheric paths for events simultaneously recorded from, at least, two different locations (Ceplecha, 1987). Approximating the meteor as a straight line, this corresponds to bearing of N309°E, incidence angle of 57° from the horizontal, and total length of the luminous trajectory of 96 km. Accordingly, the seismically estimated source height of 38.4 km corresponds to a position of 37.519°N and 3.960°W along the trajectory, comparing favorably with the seismic location (Figure 3).

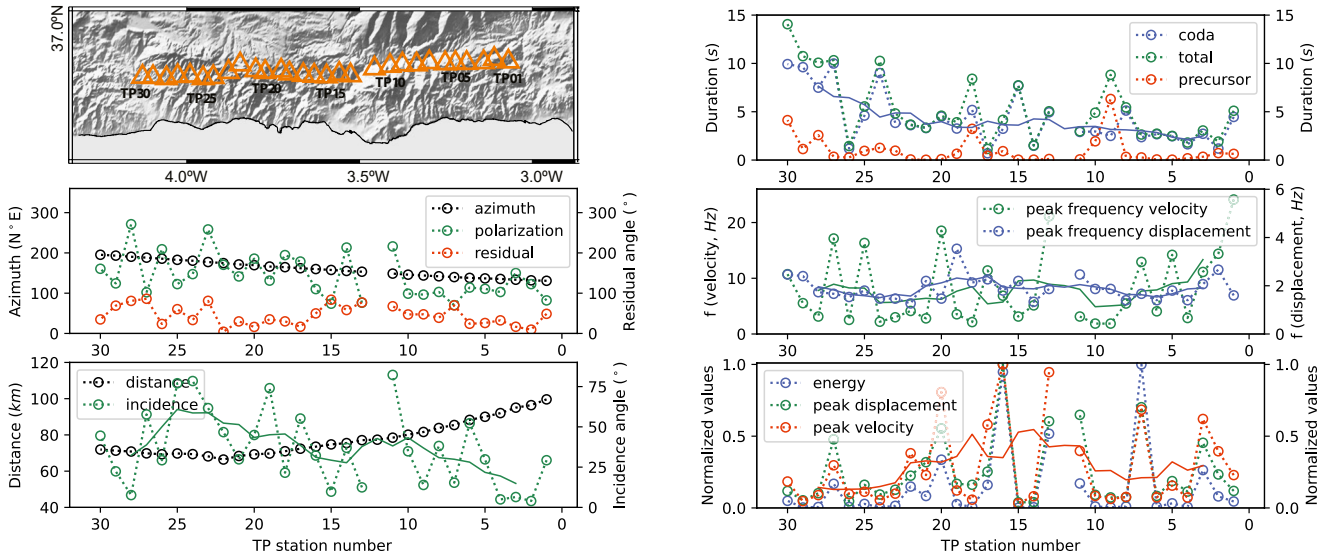

Figure 4. Station map of the Tropical Profile (TP) and characteristics of the recordings versus station number. The measured horizontal polarization and incidence of the signals (Flinn, 1965, Figure S2 in Supporting Information S1) is compared to the station azimuth and distance from the inverted location of the disintegration event. Signal duration, coda duration and precursor duration have been measured on envelope waveforms (Figure S1 in Supporting Information S1). We show frequencies of the spectral peak from velocity and displacement waveforms, as well as the signal energy from integration of squared velocity waveforms, the peak velocity amplitude, and the peak displacement amplitude. Dotted lines connect the observables pointwise, and solid lines in the same color show a moving average over five data points.

4. Source, Path and Site Effects

So far, the analysis could clarify the origin of the incoming acoustic signal from an explosive fragmentation event at 38 km height, that transfers meteoroid kinetic energy to a quasi-spherical shock wave (Edwards et al., 2008). Direct coupled waves are generated by local loading on the surface, preserving the original N-shape of pressure variations of the acoustic arrivals (Figure 1). To identify the source signal, we turn our attention to the least complex records available (e.g., TP04, TP11, TP27, Figure S1 in Supporting Information S1), which are dominated by one single N-wave. This implies that only one of the optically recorded fragmentation events was significantly involved in acoustic wave generation, presumably the most luminous event at 21:25:47.3 UTC, which also agrees with the inverted origin time. It also implies that more complex waveforms and multiple N-wave arrivals at other stations cannot be attributed to the source, but must represent propagation effects. The registration of the Granada meteor event at stations with only ∼3.5 km spacing along the Tropical Profile offers an unique opportunity to evaluate the variability of the recordings over short distances, and to discover the contribution of local propagation and coupling effects to the acousto-seismic wavefield at the Earth's surface.

To summarize the waveform characteristics along the transect, we measure signal strength, duration and spectral characteristics on vertical component waveforms, and instantaneous signal polarization from three-component velocity records (Figure 4). Polarization analysis confirms that principal arrivals are usually associated with a distinct particle motion (Figure S2 in Supporting Information S1). However, we observe large discrepancies between the geometric station azimuth and the horizontal signal polarization, corresponding to a mean absolute residual of 43°, close to the expected value for a uniform distribution of angles. Unlike some previous meteor examples (Langston, 2004; Pujol et al., 2005; D'Auria et al., 2006), the acousto-seismic polarizations of the 2016 Granada meteor do not reproduce an outward propagating pressure front. An instructive example for complexity is the recording TP22, characterized by two bundles of N-waves (Figure S2 in Supporting Information S1). The first bundle shows polarization of N170°E, close to the station azimuth of N175°E. The second bundle shows a clearly different, NE-SW polarization (N51°E) and can be attributed to an echo, possibly reflected from topography SW of the station. The contribution of echoes to signal complexity may be significant along the entire Tropical Profile due to the rugged topography of the South-Central Betics. The inclination of particle motion is also highly variable between stations, but shows a tendency toward more vertical motion for larger distances (Figure S3 in Supporting Information S1). This may point to the appearance of diffracted waves, with more vertical incidence, at the edge of the shadow zone.

Large variability of more than one order of magnitude is observed in the measurements of peak displacement, peak frequency and amplitude of velocity waveforms, and signal duration, of which only the signal duration shows a long wavelength component to the variations (Figure 4). Longer durations are found at the western stations (Figure S3 in Supporting Information S1). The gradual variation points to a path effect, where atmospheric heterogeneity in temperature and wind speed is responsible for scattering and delay of the wavefield. Multipathing through the atmospheric fine-scale structure, producing a bundle of nearby ray with similar travel times, has been previously proposed as the dominant mechanism to explain signal complexity and durations longer than the individual N-pulses (Green et al., 2011; Hedlin & Walker, 2013). Different stations present energy at different frequencies, corroborating the site dependence of the frequency characteristics of the acoustic-seismic coupling (Edwards et al., 2009). Site effects on seismoacoustic coupling may also be influenced by man-made structures (Kanamori et al., 1991), which is apparently observed at station TP07, where a standing acoustic wave between buildings can be the origin of a harmonic signal with frequency of ∼13 Hz (Figure S1 in Supporting Information S1). At many stations, the seismic signals include significant energy in the audible range (Figure 4), consistent with eyewitness (or earwitness) reports of audible sound.

The most stable waveform parameter is the peak frequency of displacement waveforms, showing values close to 2 Hz for most recordings (Figure 4). This finding reflects that displacement waveforms are constructed from individual N-wave arrivals with signal duration close to 0.5 s (Figure 1). Waveform complexity is produced principally through the repetitions of N-waves from multipathing of the acoustic wave. The variability among waveforms from the broadband transect indicates strong site effects to acousto-seismic coupling, affecting the amplitude and frequency characteristics of direct coupling and the efficiency of precursor generation, as well as site effects to multipathing. The broadband transect is located within the Alpujarride complex of the Betic mountain range, mainly composed of schists, phyllites and Mesozoic carbonate rocks (Martínez-Martínez & Azañón, 2002), with P-wave speed above 4 km/s at shallow depths (Chourak et al., 2005). All stations avoid unconsolidated sediments, yet near-surface wave speed may vary between stations, the detailed investigation of which is beyond the scope of this letter. Also topography may be effective to intensify the acousto-seismic coupling (Kanamori et al., 1992). Given the absence of other obstacles at many sites, topography is also the most plausible origin of local multipathing, augmenting the acousto-seismic waveforms with acoustic echoes.

5. Conclusions

The seismic signals recorded in southern Spain shortly after the 2016 meteor event show slow (∼0.4 km/s) apparent velocity across the network and the presence of N-shaped displacement pulses, indicating an origin from an atmospheric shock wave. We report 44 near-field detections, showing arrival times consistent with a point source at 38 km height, according to acoustic raytracing based on the ERA5 atmospheric reanalysis. The interaction between the 2016 Granada meteoroid and the atmosphere was also observed as a luminous trail starting at 98.7 km height. We can associate the origin time of the wavefield with the moment of maximum meteor luminosity, and confirm the seismic location of the principal fragmentation event by triangulation from regional meteor cameras with reasonable agreement. The remaining discrepancy could be introduced by uncertainties in the atmospheric model, or the effects of diffractions that propagate into the geometrical shadow zone. No seismic coupling has been found for the ballistic shock wave from the meteoroid passage.

The relatively large number of near-field records has been obtained due to the temporary operation of a seismic broadband transect within the detection zone. Waveforms along the dense transect illustrate the heterogeneity of the acousto-seismic wavefield, providing support for previous studies that emphasize the complexity of wave propagation and coupling (e.g., Arrowsmith et al., 2007; Edwards et al., 2009; Hedlin & Walker, 2013; Kanamori et al., 1991, 1992). In particular, amplitudes and horizontal signal polarizations show large variability among stations and seem to be dominated by site effects. These findings highlight the complexity involved in restoring the original pressure amplitudes from acousto-seismic data, a lesson that likely applies not only to meteor observations but also to other infrasound wavefields. The coda duration and incidence angles show more gradual changes along the transect, pointing to an influence of path effects. A persistent characteristic of the signals is the succession of multiple N-waves, suggesting that acoustic multipathing produces the complicate waveforms. We attribute this characteristic to local topographic scattering at the receiver site as well as to multipathing through the small-scale structure of the atmosphere along the path.

Data Availability Statement

ERA5 data that support the findings of this study are publicly available from cds.climate.copernicus.eu with the identifier https://doi.org/10.24381/cds.adbb2d47. The seismic record section is available with the identifier https://doi.org/10.7910/DVN/WQQZ9A.

Acknowledgments
We want to thank the developers of free software BAM (McFadden et al., 2021), ObsPy (Megies et al., 2011), SAC (Goldstein et al., 2003), and GMT (Wessel et al., 2019). We particularly appreciate the help by Luke McFadden with usage and parameter choices in BAM. We thank the IGN for sharing data from the Spanish broadband network, and all staff and students from IAG involved in the deployment and maintenance of the Tropical Profile. Two anonymous reviewers made valuable suggestions that have been incorporated in the final version. We receive financial support by Spanish projects CGL2015-67130-C2-2-R, A-RNM-421-UGR18, PID2019-109608GB-I00, PID2019-105797GB-I00 and B-RNM-528-UGR20.

References

Antolik, M., Ichinose, G., Creasey, J., & Clauter, D. (2014). Seismic and infrasonic analysis of the major bolide event of 15 February 2013. *Seismological Research Letters*, *85*(2), 334–343. https://doi.org/10.1785/0220130061

Arrowsmith, S. J., Drob, D. P., Hedlin, M. A. H., & Edwards, W. (2007). A joint seismic and acoustic study of the Washington State bolide: Observations and modeling. *Journal of Geophysical Research*, *112*(D9), D09304. https://doi.org/10.1029/2006JD008001

Bonyadi, M. R., & Michalewicz, Z. (2017). Particle swarm optimization for single objective continuous space problems: A review. *Evolutionary Computation*, *25*(1), 1–54. https://doi.org/10.1162/EVCO_r_00180

Brown, P., Kalenda, P., Revelle, D. O., & Borovička, J. (2003). The Morávka meteorite fall: 2 interpretation of infrasonic and seismic data. *Meteoritics & Planetary Sciences*, *38*(7), 989–1003. https://doi.org/10.1111/j.1945-5100.2003.tb00294.x

Cates, J. E., & Sturtevant, B. (2002). Seismic detection of sonic booms. *Journal of the Acoustical Society of America*, *111*(1), 614–328. https://doi.org/10.1121/1.1413754

Ceplecha, Z. (1987). Geometric, dynamic, orbital and photometric data on meteoroids from photographic fireball networks. *Bulletin of the Astronomical Institutes of Czechoslovakia*, *38*, 222–234.

Ceplecha, Z., Borovička, J., Elford, W. G., ReVelle, D. O., Hawkes, R. L., Porubčan, V., & Šimek, M. (1998). Meteor phenomena and bodies. *Space Science Reviews*, *84*(3/4), 327–471. https://doi.org/10.1023/A:1005069928850

Chourak, M., Corchete, V., Badal, J., Gómez, F., & Serón, J. (2005). Shallow seismic velocity structure of the Betic Cordillera (southern Spain) from modelling of Rayleigh wave dispersion. *Surveys in Geophysics*, *26*(4), 481–504. https://doi.org/10.1007/s10712-005-7260-4

D'Auria, L., Marotta, E., Martini, M., & Ricciolino, P. (2006). Seismic and acoustic detection of a bolide airburst in the Gulf of Naples (southern Italy). *Journal of Geophysical Research*, *111*(B10), B10307. https://doi.org/10.1029/2005JB004254

Edwards, W. N., Brown, P. G., & Eaton, D. W. (2009). Frequency-dependent acoustic–seismic coupling of meteor shock waves. *Bulletin of the Seismological Society of America*, *99*(5), 3055–3066. https://doi.org/10.1785/0120080226

Edwards, W. N., Eaton, D. W., & Brown, P. G. (2008). Seismic observations of meteors: Coupling theory and observations. *Reviews of Geophysics*, *46*(4), RG4007. https://doi.org/10.1029/2007RG000253

Edwards, W. N., Eaton, D. W., McCausland, P. J., ReVelle, D. O., & Brown, P. G. (2007). Calibrating infrasonic to seismic coupling using the Stardust sample return capsule shockwave: Implications for seismic observations of meteors. *Journal of Geophysical Research*, *112*(B10), B10306. https://doi.org/10.1029/2006JB004621

Edwards, W. N., & Hildebrand, A. R. (2004). Supracenter: Locating fireball terminal bursts in the atmosphere using seismic arrivals. *Meteoritics & Planetary Sciences*, *39*(9), 1449–1460. https://doi.org/10.1111/j.1945-5100.2004.tb00121.x

Evers, L. G., & Haak, H. W. (2007). Infrasonic forerunners: Exceptionally fast acoustic phases. *Geophysical Research Letters*, *34*(10), L10806. https://doi.org/10.1029/2007GL029353

Flinn, E. A. (1965). Signal analysis using rectilinearity and direction of particle motion. *Proceedings of the IEEE*, *53*(12), 1874–1876. https://doi.org/10.1109/proc.1965.4462

Garcés, M. A., Hansen, R. A., & Lindquist, K. G. (1998). Traveltimes for infrasonic waves propagating in a stratified atmosphere. *Geophysical Journal International*, *135*(1), 255–263. https://doi.org/10.1046/j.1365-246X.1998.00618.x

Goldstein, P., Dodge, D., Firpo, M., & Lee, M. (2003). SAC2000: Signal processing and analysis tools for seismologists and engineers. In W. H. K. Lee, H. Kanamori, P. C. Jennings, & C. Kisslinger (Eds.), *The IASPEI international handbook of earthquake and engineering seismology*. Academic Press.

Green, D. N., Vergoz, J., Gibson, R., Le Pichon, A., & Ceranna, L. (2011). Infrasound radiated by the Gerdec and Chelopechene explosions: Propagation along unexpected paths. *Geophysical Journal International*, *185*(2), 890–910. https://doi.org/10.1111/j.1365-246X.2011.04975

Hedlin, M. A. H., Drob, D., Walker, K., & de Groot-Hedlin, C. (2010). A study of acoustic propagation from a large bolide in the atmosphere with a dense seismic network. *Journal of Geophysical Research*, *115*(B11), B11312. https://doi.org/10.1029/2010JB007669

Hedlin, M. A. H., & Walker, K. T. (2013). A study of infrasonic anisotropy and multipathing in the atmosphere using seismic networks. *Philosophical Transactions of the Royal Society A*, *371*(1984), 20110542. https://doi.org/10.1098/rsta.2011.0542

Heimann, S., González, Á., Wang, R., Cesca, S., & Dahm, T. (2013). Seismic characterization of the Chelyabinsk meteor's terminal explosion. *Seismological Research Letters*, *84*(6), 1021–1025. https://doi.org/10.1785/0220130042

Hersbach, H., Bell, B., Berrisford, P., Biavati, G., Horányi, A., Muñoz Sabater, J., et al. (2018). ERA5 hourly data on single levels from 1979 to present. *Copernicus Climate Change Service (C3S) Climate Data Store (CDS)*. https://doi.org/10.24381/cds.adbb2d47

Ishihara, Y., Furumoto, M., Sakai, S., & Tsukada, S. (2004). The 2003 Kanto large bolide's trajectory determined from shockwaves recorded by a seismic network and images taken by a video camera. *Geophysical Research Letters*, *31*(14), L14702. https://doi.org/10.1029/2004GL020287

Kanamori, H., Mori, J., Anderson, D. L., & Heaton, T. H. (1991). Seismic excitation by the space shuttle Columbia. *Nature*, *349*(6312), 781–782. https://doi.org/10.1038/349781a0

Kanamori, H., Mori, J., Sturtevant, B., Anderson, D. L., & Heaton, T. (1992). Seismic excitation by space shuttles. *Shock Waves*, *2*, 89–96. https://doi.org/10.1007/bf01415896

Langston, C. A. (2004). Seismic ground motions from a bolide shock wave. *Journal of Geophysical Research*, *109*(B12), B12309. https://doi.org/10.1029/2004JB003167

Le Pichon, A., Blanc, E., & Hauchecorne, A. (2010). *Infrasound monitoring for atmospheric studies*. Springer Science & Business Media.

Lin, T.-L., & Langston, C. A. (2007). Infrasound from thunder: A natural seismic source. *Geophysical Research Letters*, *34*(14), L14304. https://doi.org/10.1029/2007GL030404

Madiedo, J. M. (2014). Robotic systems for the determination of solar system materials by means of fireball spectroscopy. *Earth Planets and Space*, *66*(1), 70. https://doi.org/10.1186/1880-5981-66-70

Madiedo, J. M. (2017). Automated systems for the analysis of meteor spectra: The SMART project. *Planetary and Space Science*, *143*, 238–244. https://doi.org/10.1016/j.pss.2016.12.005

Martínez-Martínez, J. M., & Azañón, J. M. (2002). Orthogonal extension in the hinterland of the Gibraltar Arc (Betics, SE Spain). In G. Rosenbaum & G. S. Lister (Eds.), *Reconstruction of the evolution of the Alpine-Himalayan Orogen*, *Journal of the Virtual Explorer* (Vol. *8*, pp. 1–20).

McFadden, L., Brown, P., Vida, D., & Spurný, P. (2021). Fireball characteristics derivable from acoustic data. *Journal of Atmospheric and Solar-Terrestrial Physics*, *216*, 105587. https://doi.org/10.1016/j.jastp.2021.105587

Megies, T., Beyreuther, M., Barsch, R., Krischer, L., & Wassermann, J. (2011). ObsPy – What can it do for data centers and observatories? *Annales Geophysicae*, *54*(1), 47–58.

Pierce, A. D. (2019). *Acoustics: An introduction to its physical principles and applications* (3rd ed., p. 768). Acoustical Society of America, Springer.

Pujol, J., Rydelek, P., & Bohlen, T. (2005). Determination of the trajectory of a fireball using seismic network data. *Bulletin of the Seismological Society of America*, *95*(4), 1495–1509. https://doi.org/10.1785/0120040155

Schneider, F. M., Fuchs, F., Kolínsk, P., Caffagni, E., Serafin, S., Dorninger, M., et al. (2018). Seismoacoustic signals of the Baumgarten (Austria) gas explosion detected by the AlpArray seismic network, Earth planet. *Science Letter*, *502*, 104–114.

Shewchuk, J. R. (1996). *Triangle: Engineering a 2D quality mesh generator and Delaunay triangulator, First workshop on applied computational geometry* (pp. 124–133). ACM.

Tatum, J. (1999). Fireballs: Interpretation of airblast data. *Meteoritics & Planetary Sciences*, *34*(4), 571–585. https://doi.org/10.1111/j.1945-5100.1999.tb01364.x

Virieux, J., Garnier, N., Blanc, E., & Dessa, J.-X. (2004). Paraxial ray tracing for atmospheric wave propagation. *Geophysical Research Letters*, *31*(20), L20106. https://doi.org/10.1029/2004GL020514

Walker, K. T., Hedlin, M. A. H., de Groot-Hedlin, C., Vergoz, J., Le Pichon, A., & Drob, D. P. (2010). Source location of the 19 February 2008 Oregon bolide using seismic networks and infrasound arrays. *Journal of Geophysical Research*, *115*(B12), B12329. https://doi.org/10.1029/2010JB007863

Wessel, P., Luis, J. F., Uieda, L., Scharroo, R., Wobbe, F., Smith, W. H. F., & Tian, D. (2019). The generic mapping tools version 6. *Geochemistry, Geophysics, Geosystems*, *20*(11), 5556–5564. https://doi.org/10.1029/2019GC008515

References From the Supporting Information

Google Earth. (2022). *Torvizcon Cementary, 36.8808°N, 3.2974°W, eye alt 888m, imagery date 8/3/2019*. DigitalGlobe 2022.

Kitov, I. O., Murphy, J. R., Kusnetsov, O. P., Barker, B. W., & Nedoshivin, N. I. (1997). An analysis of seismic and acoustic signals measured from a series of atmospheric and near-surface explosions. *Bulletin of the Seismological Society of America*, *87*(6), 1553–1562. https://doi.org/10.1785/bssa0870061553